Optical spectroscopy study on pressure-induced phase transitions in the three-dimensional Dirac semimetal Cd_3As_2

E. Uykur,[1,*] R. Sankar,[2] D. Schmitz,[3] and C. A. Kuntscher[1,†]
[1]*Experimentalphysik 2, Universität Augsburg, D-86159 Augsburg, Germany*
[2]*Institute of Physics, Academia Sinica, Taipei 10617, Taiwan*
[3]*Chemical Physics and Materials Science, Universität Augsburg, D-86159 Augsburg, Germany*

(Received 31 July 2017; revised manuscript received 1 May 2018; published 17 May 2018)

We report a room-temperature optical reflectivity study performed on [112]-oriented Cd_3As_2 single crystals over a broad energy range under external pressure up to 10 GPa. The abrupt drop in the band dispersion parameter (z parameter) and the interruption of the gradual redshift of the band gap at $\sim$4 GPa confirm the structural phase transition from a tetragonal to a monoclinic phase in this material. The pressure-induced increase in the overall optical conductivity at low energies and the continuous redshift of the high-energy bands indicate that the system evolves towards a topologically trivial metallic state, although a complete closing of the band gap could not be observed in the studied pressure range. Furthermore, a detailed investigation of the low-pressure regime suggests the possible existence of an intermediate state between 2 and 4 GPa, that might be a precursor of the structural phase transition or due to the lifted degeneracy of the Dirac nodes. Several optical parameters show yet another anomaly at 8 GPa where low-temperature superconductivity was found in an earlier study.

DOI: 10.1103/PhysRevB.97.195134

I. INTRODUCTION

Three-dimensional Dirac semimetals (3DDSMs) attracted a lot of attention in recent years due to their exotic electronic states. Theoretically predicted Dirac bands have also been observed by angle-resolved photoemission spectroscopy [1–4]. The conduction and valence bands in 3DDSMs touch each other at the Dirac points in momentum space, and a linear energy dispersion has been shown along all momentum directions creating the three dimensionality in these systems. Several materials have been reported, such as Na_3Bi [1] and Cd_3As_2 [5], with fascinating 3DDSM properties as a 3D analog to two-dimensional graphene.

The 3DDSM state is protected either by time-reversal symmetry and/or inversion symmetry in addition to the rotational or nonsymmorphic symmetry, and breaking one of these symmetries might drive the system into other quantum states, such as topological insulator, Weyl semimetal, and axion insulator [6,7]. This tuning can be realized either with chemical doping and/or external effects, such as magnetic fields, external pressure, or strain. These external effects are advantageous as one can eliminate additional complications resulting from the possible impurities introduced by the chemical doping.

Among all the proposed and confirmed systems, Cd_3As_2 is one of the most studied 3DDSMs. It belongs to the (II_3-V_2)-type narrow-band semiconductors showing an inverted band structure in contrast to the other members, which made it a point of interest not only today, but also previously. Moreover, it is insensitive to air conditions hence easy to handle during the measurements. Due to its interesting band structure, optical [8] and magneto-optical [9] studies at ambient pressure have been carried out, and furthermore, electrical transport and structural studies under pressure [10–12] have been performed on this material.

Previous pressure studies found the signatures of a pressure-induced structural phase transition between 2.5 and 4 GPa from a tetragonal $I4_1/acd$ phase to a monoclinic $P2_1/c$ phase where the fourfold rotational symmetry is reduced to a twofold one. Even though the structural phase transition is confirmed by various studies, the pressure at which the phase transition occurs and/or an additional intermediate phase exists is still under debate. Existing studies [10–12] show the tetragonal phase at $\sim$2.5 GPa, whereas the monoclinic phase is reported somewhere around 4.0 GPa. However, the lack of experimental data between 2.5 and 4.0 GPa does not allow one to determine the phase-transition pressure precisely. This inaccuracy also affects the discussion of the relation between structural phase transition and the observed electrical transport properties where inconsistent observations have been reported. For instance, for one of the studies [10], the system goes into metallic-semiconducting-insulating states with increasing external pressure where the metallic to semiconducting transition coincides with the structural phase transition at 2.5 GPa. For another study [11], Cd_3As_2 shows a metallic-semiconducting-metallic behavior with increasing pressure with the metallic to semiconducting transition occurring at much lower pressure (already at 1.1 GPa) compared to the observed structural phase transition (between 2.6 and 4.67 GPa). Furthermore, for pressures above 8.5 GPa a low-temperature superconducting phase has been observed, which supports the earlier proposal of Cd_3As_2 being a candidate for topological superconductivity [3].

*Present address: 1. Physikalisches Institut, Universität Stuttgart, Germany; ece.uykur@pi1.physik.uni-stuttgart.de
†christine.kuntscher@physik.uni-augsburg.de

The inconsistent findings of earlier pressure-dependent resistivity and structural investigations motivated us to carry out a study on the charge dynamics of Cd_3As_2 under external pressure from an optical point of view. In particular, we focused on the pressure range between 2 and 4 GPa where literature data are scarce to elucidate possible new phases emerging under pressure.

II. EXPERIMENT

Large single crystals of Cd_3As_2 were synthesized with the self-selecting vapor growth method [13]. A piece with size of $250 \times 250 \times 65\ \mu m^3$ was used in the current measurements. Samples are polished down to 0.1 μm prior to measurements, and the crystallographic facet is determined as the [112] surface by x-ray diffraction (XRD). The sample is placed into a type-IIa diamond-anvil cell (DAC) [14], and finely ground CsI powder was used as a quasihydrostatic pressure transmitting medium. The ruby luminescence method was used for the pressure determination inside the DAC [15].

The pressure-dependent room-temperature reflectivity measurements were performed with a Hyperion infrared microscope which is coupled to a Bruker Vertex 80v Fourier-transform infrared spectrometer. Measurements were carried out on the same crystal piece for the entire energy range ($\sim$100–20 000 cm^{-1}). The reflectivity spectra are measured at the sample-diamond interface where a CuBe gasket was used as the reference. The intensity of the measured reflectivity was normalized by the intensity reflected from the CuBe gasket at the gasket-diamond interface. The gradual change from the ambient-pressure spectrum (taken at the sample-vacuum interface) suggests that the reference correction was reasonable.

The data around 2000 cm^{-1} are affected by the multiphonon absorption in the diamond, therefore, this energy range was cut out and interpolated using the Drude-Lorentz (DL) fitting of the reflectivity spectra for further analysis. The optical conductivity spectra were calculated from the measured reflectivity via Kramers-Kronig (KK) transformation as explained elsewhere [16].

III. RESULTS AND DISCUSSION

A schematic of the density of states (DOS) [3] and the Dirac bands of Cd_3As_2 is depicted in Fig. 1. The low-energy electrodynamics of Cd_3As_2 is determined by As 4*d* and Cd 5*s* states in the vicinity of the Fermi energy. A band

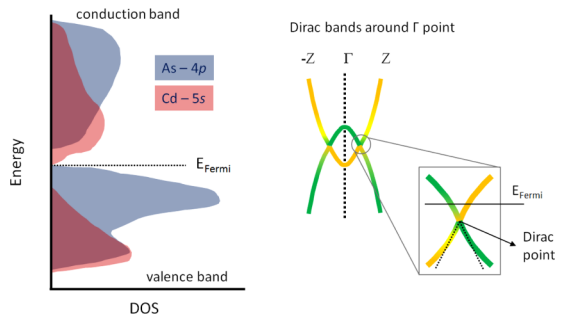

FIG. 1. Schematic of the DOS [3] and the Dirac bands of Cd_3As_2.

inversion along the Γ-Z direction can be seen in the electronic structure where one also observes Dirac bands [3]. Cd_3As_2 is a naturally doped system, therefore the Fermi energy lies in the conduction band. Moreover, the deviation from the perfectly linear dispersion of the Dirac bands in Cd_3As_2 is an issue which is discussed intensively. More details regarding this issue are given in the following parts of the paper.

In electrical transport measurements pronounced pressure-induced changes were observed for Cd_3As_2 under pressure [10–12], and therefore, one would expect to observe corresponding pressure-induced effects in optical spectra as well. In Fig. 2(a) the room-temperature reflectivity spectra are depicted for selected pressures. At the lowest pressure (1.0 GPa), a sharp plasma edge is observed at $\sim$600 cm^{-1}, which is an indication for a Drude-like response. This finding is also consistent with the metallic electrical resistivity shown for this material since the Fermi energy in Cd_3As_2 is located in the conduction band. Up to 2 GPa no significant changes are observed in the reflectivity spectra. Between 2 and 5 GPa a gradual increase in the reflectivity level above the plasma edge frequency is observed, and the sharp steplike behavior due to the appearance of the plasma edge starts to be smeared out. Above 5 GPa the increase in the reflectivity level is accompanied by a sudden disappearance of the clear plasma edge.

The corresponding real part of the optical conductivity $\sigma_1(\omega)$ obtained from the reflectivity spectra via KK transformation is given in Fig. 2(b). Up to 2 GPa an almost unchanged absorption edge at high energies is observed. Above 2 GPa a gradual shift of the absorption edge towards lower energies occurs, which is interrupted at $\sim$4 GPa, and above this pressure the continuation of the shift is visible, becoming more rapid above 8 GPa.

In Fig. 2(c) we show the low-energy optical conductivity for selected pressures. Black triangles indicate the observed phonon modes at 1.0 GPa, which are consistent with the reported ambient-pressure studies [8]. Although at room temperature the phonon modes are broad in nature, they can be distinguished, and their pressure evolution can be traced. One should note that this material shows several more phonon modes especially in the low-energy region close to our measurement limit, but due to the close proximity to the diffraction limit (due to the small sample size) we cannot separate them clearly. With increasing pressure, the increasing higher-energy spectral weight strongly masks the phonon mode at around 220 cm^{-1}. Up to 3.5 GPa the phonon spectrum is hardly changing, and above this pressure the phonon modes around 150–170 cm^{-1} are strongly suppressed. The possible appearance of new phonon modes is hard to distinguish since the spectral weight shifting towards the low-energy region tends to smear out the structures. The low-energy data are limited in the current paper due to the diffraction limit, which is generally the case for small samples in the pressure cell. However, one can note that the optical conductivity at high pressures seems to be lower compared to the low-pressure regime, although the high-energy spectral weight is increasing. On the other hand, the reflectivity spectra clearly show a Hagen-Rubens-like frequency dependence indicating the existence of free carriers at high pressures as well. This finding suggests the existence of a narrow Drude component at high pressures which is probably out of our measurement range. In the inset of the

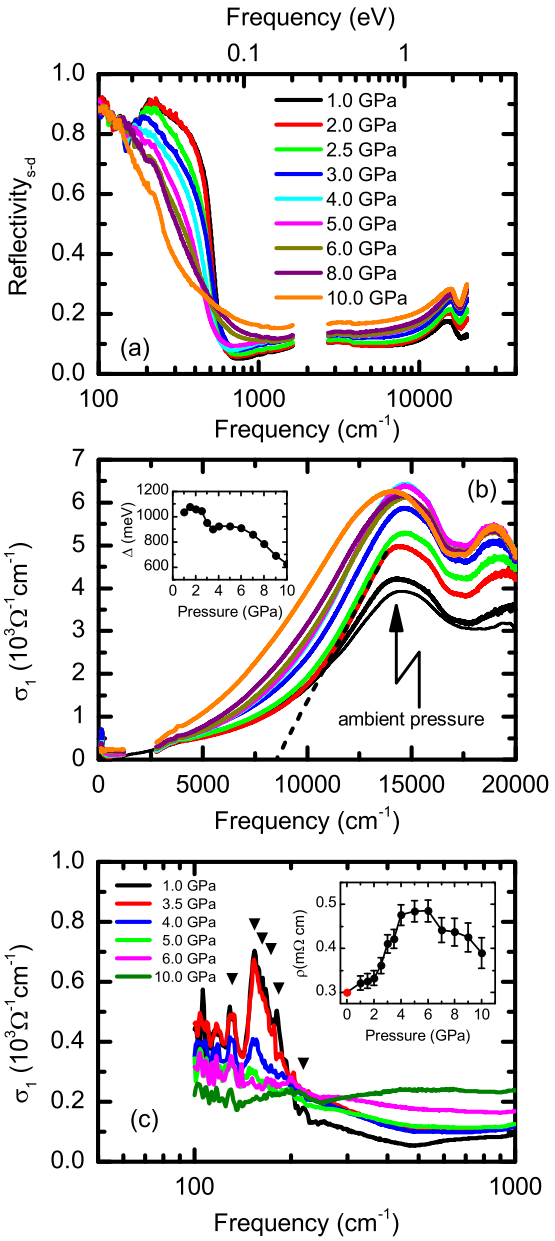

FIG. 2. Pressure-dependent (a) reflectivity and (b) optical conductivity σ_1 of Cd_3As_2. The inset: Pressure dependence of the high-energy band-gap Δ determined by a linear extrapolation of the absorption edge to the frequency axis. An example for the linear fit (dashed line) is shown for the optical conductivity data at 2 GPa. The ambient-pressure conductivity spectrum taken at the vacuum-sample interface with an aluminum mirror as a reference is given for comparison. (c) Low-energy optical conductivity spectrum of Cd_3As_2 for selected pressures. Triangles indicate the phonon modes at 1.0 GPa. The inset shows the dc-resistivity values extracted from the current study. The ambient-pressure data point from Ref. [11] is included for comparison with the literature data.

Fig. 2(c) we plotted the dc-resistivity values extracted from the current study ($\rho_{dc} = 1/\sigma_{1,\omega\to 0}$) with the dc-resistivity value taken from Ref. [11] for a comparison at ambient pressure. The increasing resistivity with increasing pressure in the low-pressure regime is consistent with the previous studies. Moreover, the saturation and slight decrease in the resistivity in the higher-pressure range, i.e., above 4 GPa, indicate that the metallicity of the system starts to be increased which is in similar lines with a previous study [11] as well.

The interband conductivity in 3DDSM systems is expected [17,18] to show a specific behavior. The optical conductivity should follow a universal power-law frequency dependence according to $\sigma_1(\omega) \propto \omega^{(d-2)/z}$. Here d is the dimensionality of the system, and z can be obtained from the band dispersion relation $E(k) \propto |k|^z$. By using these relations, one would expect to observe an ω-linear optical conductivity for a 3DDSM. Such behavior of the optical conductivity has indeed been shown for several materials, such as quasicrystals [19] and $ZrTe_5$ [20].

For Cd_3As_2, on the other hand, a sublinear dispersion is expected as discussed theoretically and shown by experimental probes [5,21–23]. In the very low-energy region close to the Dirac points, it is expected that this sublinear dispersion eventually evolves to a linear one. However, it is a difficult task to observe or extract this ω-linear behavior since the existence of free charge carrier in the system shifts the Fermi energy above the Dirac point and the plasma edge behavior masks the ω-linear region. More elaborate models have been proposed for doped 3DDSMs, which take into account the shift of the Fermi energy, etc., although they do not account for the sublinear dispersion [24–26]. However, for the Cd_3As_2 samples, optical studies showed a Dirac cone Pauli-blocked edge at around 1700 cm^{-1}, which implies a Fermi level around 100 meV, also consistent with the literature regarding the reported carrier concentrations [27]. In our measurement, the energy range between 1600 and 2500 cm^{-1} is affected by the multiphonon absorption of the diamond, and therefore, it is impossible for us to employ and discuss the mentioned theories. Hence, we analyzed our data with a simplified $\sigma_1(\omega) \propto \omega^{1/z}$ approach [19], which we believe will show the general behavior of the pressure evolution.

In Fig. 3(a) the fitting of the optical conductivity for 1 and 10 GPa is depicted as examples. Fittings have been performed in the frequency range of 4000–6000 cm^{-1} for all pressures. The small peaklike features around 4000 cm^{-1} are also due to multiphonon absorption in the diamond anvil. In Fig. 3(b) the value of the z parameter, as extracted by the fitting, is given as a function of pressure. The pressure range can be divided into two distinct regimes. In the low-pressure regime, the z parameter has a value around 0.8 and does not show a significant change with increasing pressure within the error bars. Moreover, the values lower than 1 confirm the sublinear behavior of the band dispersion. With increasing pressure above 4 GPa, lower values for the z parameter, which is almost unchanged in the high-pressure regime, is observed indicating the flattening of the bands. The question arises whether the low-pressure Dirac state survives above 4 GPa or not. The phase in the pressure range above the structural phase transition was specified as semiconducting based on the electrical transport measurements, and a band gap has been determined. However, such a gap opening at Dirac bands does not contradict with the possibility of the survival of the Dirac bands [8,25,28].

Previous electrical transport measurements reported contradictory interpretations of the high-pressure phase in Cd_3As_2. In one of these studies [10] it has been proposed that the system

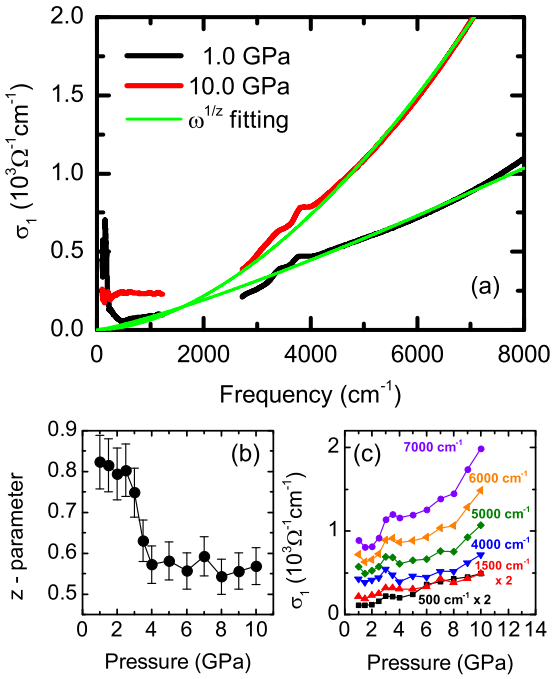

FIG. 3. (a) Optical conductivity σ_1 and $\omega^{1/z}$ fittings at 1.0 and 10 GPa. The small absorption features around 4000 cm^{-1} are due to multiphonon excitations in the diamond anvil. Fittings were performed in the frequency range of 4000–6000 cm^{-1}. (b) Value of the z parameter, which is a measure of the band dispersion, as a function of pressure as extracted by the fitting. (c) Pressure dependence of σ_1 at various frequencies. The data at 500 and 1500 cm^{-1} were multiplied by a factor of 2 for clarity.

undergoes a structural phase transition at around 2.5 GPa where above this pressure the Dirac state is broken and a gradual increase in the resistivity indicates the semiconducting (and insulating with a further increase in pressure) nature of the system. Another resistivity and XRD study [11] confirmed the pressure-induced transition to a monoclinic structure and to a semiconductor-like electrical resistivity and found a metallic state above 8.5 GPa with superconductivity at low temperatures. The latter finding was discussed from the topological insulator state point of view where one would also expect topological superconductivity. Our results do not completely exclude the conclusions drawn by the mentioned publications, however, a different interpretation for the high-pressure regime might be necessary.

Signatures of a pressure-induced structural phase transition can also be found in the optical spectra, namely, an anomaly is observed at 4 GPa in several optical parameters: (i) The disappearance of several phonon modes [Fig. 2(c)] suggests a structural phase transition. (ii) The drop of the z parameter [Fig. 3(b)] indicates a sudden change in the band structure, which can be due to the breakdown of the fourfold rotational symmetry. (iii) The gradual redshift of the high-energy band gap [see the inset of Fig. 2(b)] is interrupted at 4 GPa. The latter indicates that the changes happening at this pressure are sensed by the whole electronic band structure and not only by the Dirac bands, which support the structural nature of the observed changes at this pressure. Furthermore, the shift of the high-energy bands towards lower energies (especially above 8 GPa) with an increase in the conductivity level at low energies [see Fig. 3(c)] indicates that the system does not show an insulating behavior in contrast to Ref. [10] but rather evolves towards a metallic state. Hence, the results of our paper are more consistent with the findings in Ref. [11]. Please note that the band gap is not completely closed, and thus a completely metallic state was not observed within the measured pressure range.

A more detailed investigation of the low-pressure regime reveals that there might be a pressure-induced intermediate phase before the occurrence of the structural phase transition at 4 GPa. In Fig. 3(c), the values of $\sigma_1(\omega)$ are plotted at various frequencies as a function of pressure. To rule out possible effects of the phonon modes, the frequencies were chosen in the energy range above the phonon contributions. At each frequency an anomaly in the optical conductivity is visible between 2 and 4 GPa. It is a rather ambiguous process to determine the exact pressure at which the structural phase transition occurs. Previous XRD studies provide data at 2.42 GPa [10] and 2.60 GPa [11] and show that the system is in a tetragonal phase, whereas the next measured pressure step was only at 3.78 and 4.67 GPa, respectively, where the high-pressure monoclinic phase was reported. The large pressure step between these two phases prevents a clear determination of the phase-transition pressure. This might, however, be important to clarify the existence of an intermediate phase. We point out that in Ref. [10] a kink behavior of the Hall resistance was observed at 2.09 GPa, which might indicate the existence of an intermediate state. Moreover, a recent XRD study [12] also presents data with seemingly a mixed phase at 2.92 GPa, but unfortunately a discussion of this phase has not been given.

Hints for an intermediate phase between 2 and 4 GPa can be found in other optical variables as well. In Fig. 4 we present the fitting of the reflectivity at several pressures as examples [Fig. 4(a)], and the so-obtained spectral weight (SW) and scattering rate $(1/\tau)$ for the observed Drude component are plotted as well [Figs. 4(b) and 4(c), respectively]. To obtain a better accuracy, the fittings have been performed simultaneously on reflectivity and optical conductivity data up to 1500 cm^{-1}, which is well above the observed plasma edge. Moreover, the fitting was repeated up to 20 000 cm^{-1} by taking into account the much higher-lying bands. A sudden increase in the SW is observed at 2 GPa, which could be associated with a SW transfer from the high-energy interband transitions to the low-energy intraband Drude component. Such a SW transfer could be interpreted in terms of a splitting of the degenerate Dirac nodes to a Weyl semimetal phase in the framework of the Dirac fermions [25]. Concurrent with the structural phase transition the rotational symmetry in Cd_3As_2 is reduced. However, if an intermediate state exists, then it is also possible that the inversion symmetry will be disturbed by external pressure prior to the rotational symmetry lowering, which will result in a Dirac semimetal-to-Weyl semimetal transition. Furthermore, the observed anomalous behavior between 2 and 4 GPa might only be a precursor of the structural phase transition.

The anomalies found for the parameters of the Drude component [Figs. 4(b) and 4(c)] are not affected by the high-energy bands and the phonon modes as shown in the following. To this end, we plot the Drude + Lorentz fittings for

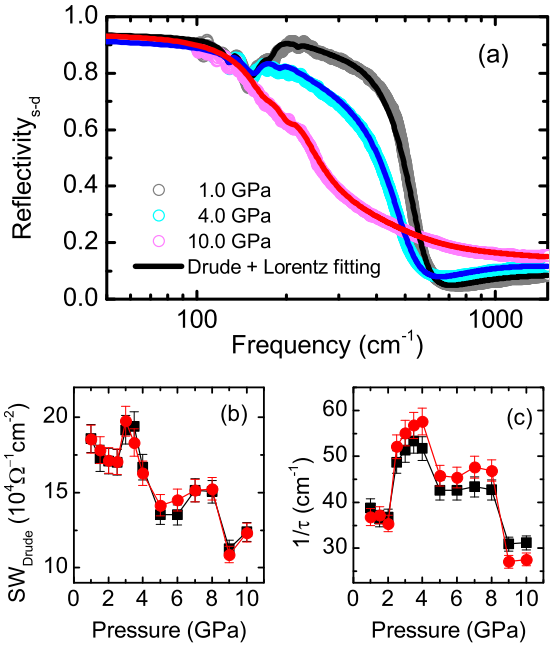

FIG. 4. (a) Reflectivity and DL fitting of the measured reflectivity at 1.0, 4.0, and 10 GPa. (b) Spectral weight and (c) scattering rate of the Drude component obtained from the fittings. Results from the fittings up to 1500 and 20 000 cm^{-1} are indicated by solid squares and solid circles, respectively.

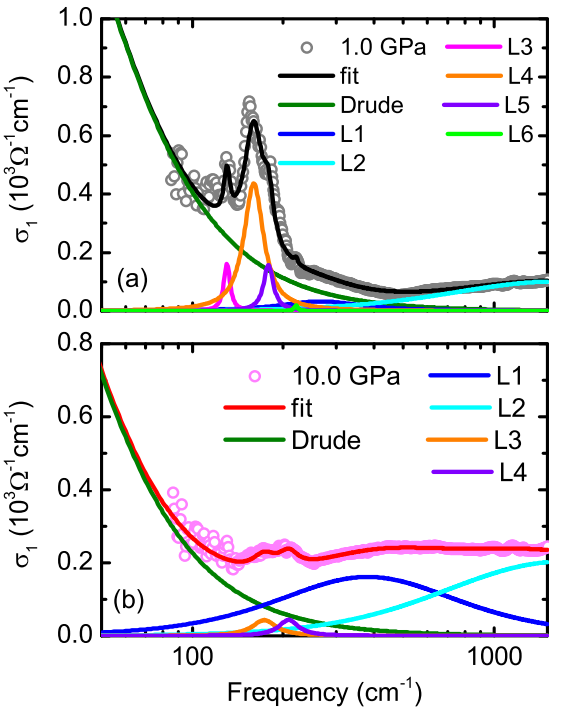

FIG. 5. Optical conductivity and DL fitting at (a) 1.0 GPa and (b) 10.0 GPa with the following components: Drude, L1, and L2 for the high-energy contributions and L3–L6 for the phonon contributions.

the optical conductivity spectra with the fitting contributions at 1.0 and 10.0 GPa in Figs. 5(a) and 5(b), respectively. Here, the Lorentz terms L1 and L2 reflect the high-energy contributions where one can see a significant increase in their SW with increasing pressure, demonstrating the increase in the reflectivity and the optical conductivity mentioned above. Moreover, at 1.0 GPa very clear phonon modes can be resolved labeled as L3–L6. Please note that L4 can in principle be separated into three different phonon modes as shown in Fig. 2(c) (also as in line with the literature), however, for simplicity, we just assumed one contribution with a larger width. With increasing pressure the phonon modes are smeared out, and only two of the four phonon modes are visible within the resolution of our spectra. Moreover, the SW contributions of these phonon modes are also significantly weakened under pressure. Due to the small and confined SW of the phonon modes, both at low and at high pressures, these phonon modes do not affect the Drude scattering rate. On the other hand, the high-energy contributions might have more prominent effects. For the low-pressure regime, the L1 and L2 contributions are small enough so that their low-energy contributions can be ignored. For the high-pressure regime, these two contributions grow significantly, and it becomes difficult to distinguish these modes from the Drude one (plasma edge in reflectivity is smeared out). The L2 term is still in the high-energy regime so that it can be well separated from the Drude mode. The tail of the L1 mode can, in principle, affect the choice of the scattering rate of the Drude mode. Therefore, the possible choices of the fitting parameters for the Drude mode are given as error bars in Figs. 4(b) and 4(c). With the given error bars, the anomalies in the pressure-dependent Drude parameters are clearly visible.

Another interesting point of the presented data is the evolution of the plasma edge, which is illustrated by the loss function (Fig. 6). The loss function is obtained from the dielectric function $\epsilon(\omega)$ as $-\mathrm{Im}[1/\epsilon(\omega)]$. At the lowest pressure, the loss function shows a clear maximum at the screened plasma frequency, which confirms the plasma edge observed in reflectivity spectrum and the intraband Drude response, which is expected in this naturally doped system (Fermi energy lies in the conduction band). The width of this mode is increasing with increasing pressure and overall the mode shifts to lower energies. A Fano-like fitting [29] has been performed to obtain the peak position [inset of Fig. 6(b)], which is given as a function of pressure in Fig. 6(b). Here, one notes a small jump between 2 and 4 GPa, confirming the existence of an intermediate phase as revealed by anomalies in various optical parameters as discussed above. With a further pressure increase, it seems that the high-energy contributions superpose the clear plasma behavior, however, the existence of the free carriers is clearly revealed in the reflectivity spectra by the Hagen-Rubens upturn towards lower frequencies. At these high pressures the clear peaklike structure in the loss function disappears, and hence the peak position above 8 GPa is not discussed. This smearing out of the plasmon mode with increasing pressure is another indication that the high-energy interband transitions are pushed towards the lower-energy region and start to overlap with the low-energy excitations, indicating the increasing metallicity of the system.

The evolution of several optical parameters at the critical pressure of 8 GPa is also intriguing. Although no further structural transitions have been reported for this pressure range, we observe several anomalies in the optical spectra.

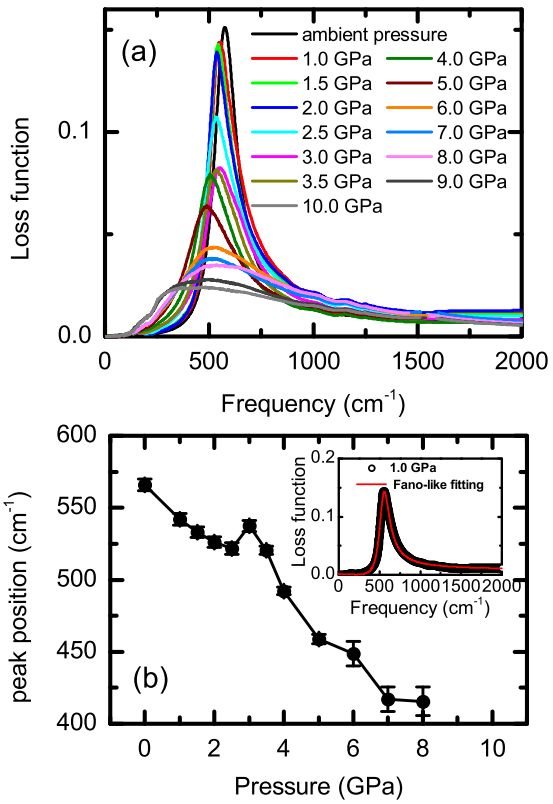

FIG. 6. (a) Pressure dependence of the low-energy loss function $-\mathrm{Im}[1/\epsilon(\omega)]$. Ambient-pressure data are included for comparison. These data were obtained at the sample-vacuum interface using an aluminum mirror as the reference. (b) Peak position of the loss function as obtained by the fitting. The inset: Example for the Fano-like fitting of the loss function at 1.0 GPa.

Namely: (i) the drop of the Drude SW and the scattering rate [Figs. 4(b) and 4(c)] followed by the increasing trend of the Drude SW, (ii) a more rapid increase in the optical conductivity at various energy ranges [Fig. 3(c)], and (iii) the broadening and disappearance of the plasmon peak in the loss function [Fig. 6(a)]. All these changes indicate that the system goes into a more metallic state above 8 GPa. We would also like to point out that this pressure range coincides with the range where low-temperature superconductivity was observed in electrical transport measurements [11].

IV. CONCLUSIONS

In conclusion, our pressure-dependent optical study of the 3DDSM Cd_3As_2 confirms the occurrence of a structural phase transition at 4 GPa in terms of anomalies in the optical spectra: (i) The z parameter of the band dispersion relation [$E(k) \propto |k|^z$] shows an abrupt drop. (ii) The redshift of the high-energy bands is interrupted. For pressures above 4 GPa the continuous redshift of the high-energy bands indicates that system goes towards a metallic state, however, a complete transition could not be observed within the measured pressure range. Moreover, the existence of a Hagen-Rubens-like reflectivity with the disappearance of the plasmon peak indicates the shift of the high-energy bands towards lower energies, which gives further evidence for the increasing metallicity of the system. For pressures between 2 and 4 GPa we observe anomalies in the optical response, for example, in the Drude parameters, which suggest the existence of an intermediate state with a possible pressure-induced splitting of the Dirac nodes and a phase transition to a Weyl semimetal state. For the clarification of the nature of this intermediate phase detailed structural studies in this pressure range are necessary. Furthermore, we find anomalies in the optical response at 8 GPa where the emergence of a low-temperature superconducting phase was observed.

ACKNOWLEDGMENTS

We thank A. A. Tsirlin and J. P. Carbotte for fruitful discussions. This project was financially supported by the Federal Ministry of Education and Research (BMBF), Germany, through Grant No. 05K13WA1 (Verbundprojekt No. 05K2013, Teilprojekt No. 1, PT-DESY).

[1] Z. Wang, Y. Sun, X.-Q. Chen, C. Franchini, G. Xu, H. Weng, X. Dai, and Z. Fang, Phys. Rev. B **85**, 195320 (2012).
[2] S. M. Young, S. Zaheer, J. C. Y. Teo, C. L. Kane, E. J. Mele, and A. M. Rappe, Phys. Rev. Lett. **108**, 140405 (2012).
[3] Z. Wang, H. Weng, Q. Wu, X. Dai, and Z. Fang, Phys. Rev. B **88**, 125427 (2013).
[4] T. Wehling, A. Black-Schaffer, and A. Balatsky, Adv. Phys. **63**, 1 (2014).
[5] M. Neupane, S.-Y. Xu, R. Sankar, N. Alidoust, G. Bian, C. Liu, I. Belopolski, T.-R. Chang, H.-T. Jeng, H. Lin, A. Bansil, F. Chou, and M. Z. Hasan, Nat. Commun. **5**, 3786 (2014).
[6] W. Witczak-Krempa, G. Chen, Y. B. Kim, and L. Balents, Annu. Rev. Condens. Matter Phys. **5**, 57 (2014).
[7] B. Yang and N. Nagaosa, Nat. Commun. **5**, 4898 (2014).
[8] D. Neubauer, J. P. Carbotte, A. A. Nateprov, A. Löhle, M. Dressel, and A. V. Pronin, Phys. Rev. B **93**, 121202 (2016).
[9] A. Akrap, M. Hakl, S. Tchoumakov, I. Crassee, J. Kuba, M. O. Goerbig, C. C. Homes, O. Caha, J. Novák, F. Teppe, W. Desrat, S. Koohpayeh, L. Wu, N. P. Armitage, A. Nateprov, E. Arushanov, Q. D. Gibson, R. J. Cava, D. van der Marel, B. A. Piot, C. Faugeras, G. Martinez, M. Potemski, and M. Orlita, Phys. Rev. Lett. **117**, 136401 (2016).
[10] S. Zhang, Q. Wu, L. Schoop, M. N. Ali, Y. Shi, N. Ni, Q. Gibson, S. Jiang, V. Sidorov, W. Yi, J. Guo, Y. Zhou, D. Wu, P. Gao, D. Gu, C. Zhang, S. Jiang, K. Yang, A. Li, Y. Li, X. Li, J. Liu, X. Dai, Z. Fang, R. J. Cava, L. Sun, and Z. Zhao, Phys. Rev. B **91**, 165133 (2015).
[11] L. He, Y. Jia, S. Zhang, X. Hong, C. Jin, and S. Li, Quantum Materials **1**, 16014 (2016).
[12] C. Zhang, J. Sun, F. Liu, A. Narayan, N. Li, X. Yuan, Y. Liu, J. Dai, Y. Long, Y. Uwatoko, J. Shen, S. Sanvito, W. Yang, J. Cheng, and F. Xiu, Phys. Rev. B **96**, 155205 (2017).

[13] R. Sankar, M. Neupane, S.-Y. Xu, C. J. Butler, I. Zeljkovic, I. P. Muthuselvam, F.-T. Huang, S.-T. Guo, S. K. Karna, M.-W. Chu, W. L. Lee, M.-T. Lin, R. Jayavel, V. Madhavan, M. Z. Hasan, and F. C. Chou, Sci. Rep. **5**, 12966 (2015).
[14] R. Keller and W. B. Holzapfel, Rev. Sci. Instrum. **48**, 517 (1977).
[15] H. K. Mao, J. Xu, and P. M. Bell, J. Geophys. Res. **91**, 4673 (1986).
[16] A. Pashkin, M. Dressel, and C. A. Kuntscher, Phys. Rev. B **74**, 165118 (2006).
[17] P. Hosur, S. A. Parameswaran, and A. Vishwanath, Phys. Rev. Lett. **108**, 046602 (2012).
[18] A. Bácsi and A. Virosztek, Phys. Rev. B **87**, 125425 (2013).
[19] T. Timusk, J. P. Carbotte, C. C. Homes, D. N. Basov, and S. G. Sharapov, Phys. Rev. B **87**, 235121 (2013).
[20] R. Y. Chen, S. J. Zhang, J. A. Schneeloch, C. Zhang, Q. Li, G. D. Gu, and N. L. Wang, Phys. Rev. B **92**, 075107 (2015).
[21] S. Borisenko, Q. Gibson, D. Evtushinsky, V. Zabolotnyy, B. Büchner, and R. Cava, Phys. Rev. Lett. **113**, 027603 (2014).
[22] Z. K. Liu, J. Jiang, B. Zhou, Z. J. Wang, Y. Zhang, H. M.Weng, D. Prabhakaran, S.-K. Mo, H. Peng, P. Dudin, T. Kim, M. Hoesch, Z. Fang, X. Dai, Z. X. Shen, D. L. Feng, Z. Hussain, and Y. L. Chen, Nat. Mater. **13**, 677 (2014).
[23] S. Jeon, B. B. Zhou, A. Gyenis, B. E. Feldman, I. Kimchi, A. C. Potter, Q. D. Gibson, R. J. Cava, A. Vishwanath, and A. Yazdani, Nat. Mater. **13**, 851 (2014).
[24] P. E. C. Ashby and J. P. Carbotte, Phys. Rev. B **89**, 245121 (2014).
[25] C. J. Tabert, J. P. Carbotte, and E. J. Nicol, Phys. Rev. B **93**, 085426 (2016).
[26] C. J. Tabert and J. P. Carbotte, Phys. Rev. B **93**, 085442 (2016).
[27] G. S. Jenkins, C. Lane, B. Barbiellini, A. B. Sushkov, R. L. Carey, F. Liu, J. W. Krizan, S. K. Kushwaha, Q. Gibson, T.-R. Chang, H.-T. Jeng, H. Lin, R. J. Cava, A. Bansil, and H. D. Drew, Phys. Rev. B **94**, 085121 (2016).
[28] T. Morimoto and N. Nagaosa, Sci. Rep. **6**, 19853 (2016).
[29] U. Fano, Phys. Rev. **124**, 1866 (1961).